

Article

Collision-Free Formation-Containment Control Based on Adaptive Sliding Mode Strategy for a Quadrotor Fleet Under Disturbances

Carlos Katt  and Herman Castañeda  *

Tecnológico de Monterrey, School of Sciences and Engineering, Av. Eugenio Garza Sada 2501 Sur, Col. Tecnológico, Monterrey 64849, NL, Mexico

* Correspondence: hermancc@tec.mx

Highlights

What are the main findings?

- The controller is based on adaptive sliding mode control to ensure finite-time convergence under uncertainties.
- Practical finite-time performance was demonstrated through Lyapunov-based stability analysis.

What is the implication of the main finding?

- Enables robust control without overestimating gains, improving efficiency and adaptability.
- Provides a scalable framework for formation control with integrated inter-agent collision avoidance.

Abstract

This manuscript presents a robust formation and collision-free containment control system designed for a quadrotor fleet operating under turbulent wind conditions. Emphasizing collision avoidance, we introduce a two-layer strategy in which a virtual leader defines a trajectory, and leaders and followers maintain their positions while avoiding collisions among them. A graph convention is used to illustrate the roles of leaders and followers, as well as their interactions. Inter-agent collision avoidance is proposed by expanding the desired distance relative to all neighboring agents, thereby guaranteeing the convergence stage. Moreover, the approach employs a class of adaptive sliding mode strategies to ensure finite-time convergence, as well as non-overestimation of the control gain in the presence of uncertainties and perturbations. A stability analysis demonstrates the practical finite-time stability of the system using the Lyapunov methodology. Results from the simulation underscore the effectiveness of our proposal in adhering to the desired time-varying trajectories and ensuring sensor-less inter-agent collision avoidance for the followers, even in the presence of turbulent wind conditions.



Academic Editors: Kaiyu Qin, Haitao Nie, Jinliang Shao, Lei Shi, Mengji Shi, Boxian Lin and Yang Zhu

Received: 20 August 2025

Revised: 14 October 2025

Accepted: 15 October 2025

Published: 18 October 2025

Citation: Katt, C.; Castañeda, H. Collision-Free Formation-Containment Control Based on Adaptive Sliding Mode Strategy for a Quadrotor Fleet Under Disturbances. *Drones* **2025**, *9*, 724. <https://doi.org/10.3390/drones9100724>

Copyright: © 2025 by the authors. Licensee MDPI, Basel, Switzerland. This article is an open access article distributed under the terms and conditions of the Creative Commons Attribution (CC BY) license (<https://creativecommons.org/licenses/by/4.0/>).

Keywords: quadrotor fleet; formation-containment; adaptive sliding control; multi-agents; collision-free

1. Introduction

Recently, the incorporation of robotics into social functions has garnered significant attention, leading to the practical deployment of multi-robot systems in diverse areas, including entertainment, agricultural automation, and defense applications [1]. This surge

in interest has prompted significant attention towards cooperative robotic systems, which present complex challenges, notably in guiding these robotic ensembles effectively toward their intended objectives. Cooperative control is the key to ensuring seamless interaction and coordination between system components, enabling the successful navigation of the environment and execution of tasks. Rotary-wing unmanned aerial vehicles (UAVs), with their inherent stability, vertical take-off and landing capabilities, and precise hovering abilities, exemplify the potential of such systems, particularly in tasks such as surveillance, inspection, and target tracking [2]. Thus, interest in cooperative robotics continues to expand across various sectors, including agriculture [3], industrial production [1], and inventory management [4]. The versatility of UAVs has been increasingly recognized for their ability to cover expansive territories and access remote or challenging locations.

In light of this, as the number of robots interacting with each other increases, we see an escalation in system complexity and data load. Distributed control strategies, such as consensus, containment, and formation control, provide an effective solution to mitigate these challenges. Consensus algorithms enable all agents in a network to agree on a common state using only the information exchanged through the communication network, as elaborated in [5,6]. In systems without defined leaders, the primary control objective is to ensure consensus formation on the estimated states of the neighboring elements of the system, as discussed in [7–9].

The leader–follower approach helps to manage the amount of information shared within a system. For instance, in situations requiring constant communication with a base of operations, limiting the number of agents who send or receive data can prevent communication overload. To achieve this, a smaller group of agents is designated as the leaders. These leaders receive trajectory information and guide the rest of the agents, considered followers, through a consensus process. Several issues have been identified in this kind of system—such as convergence coordination in [10]—when considering uncertainties in the trajectory and the system in [11], addressing communication reliability [12–14], robustness to disturbances [15], and control of heterogeneous systems [16]. Given the complexity inherent in multi-agent system applications, effective task execution necessitates adaptive and dynamic interactions among the agents. When multiple leaders are used to define the shape of the formation, this is known as containment control. In this setup, followers do not send information back to leaders, meaning that the consensus does not directly control the leaders; instead, it uses them as reference points. This introduces uncertainty, especially when guiding followers through dynamic formations or unfamiliar paths. Regardless of this new challenge, the flexibility to transmit information exclusively to leaders and adjust the formation as required provides significant advantages. Hence, the formation-containment strategy offers a more practical implementation by directing the leaders to achieve a predefined formation while ensuring that the followers remain confined within the convex hull defined by the leaders. In [17,18], a dynamic strategy for implementing formation-containment control in linear multi-agent systems is proposed. Reacting to the environment presents the problem of formation, which changes over time, as a crucial topic [19].

Implementing UAV systems in confined indoor environments presents challenges, including size limitations and a high risk of collisions with obstacles. Micro air vehicles (MAVs) are well-suited for such settings due to their compact design. Still, their limited size and weight restrict the integration of complex sensor systems within a single unit. In addition, MAVs are highly sensitive to external disturbances. When multiple agents operate in the same space, the risk of mutual interference increases significantly. As a result, robust solutions are crucial for effectively managing external perturbations and system uncertainties. Adaptive control schemes have been investigated to effectively address this

issue in linear systems, particularly in first- and second-order multi-agent systems [20–23]. However, they often fail to consider the full dynamics of the agents and do not account for perturbations.

Another challenging issue when working with multi-agent systems is the need for agents to avoid collisions with one another. As with numerous MAVs, the possibility of collision poses a significant threat that could result in the loss of multiple agents. Solutions to coordinate trajectories and avoid collisions of low-complexity multi-agent systems were presented in [24–26]. In [27,28], the formation problem of multi-agent systems was studied while avoiding collision, but perturbations were not considered.

This paper presents a novel and robust formation-containment control framework for a fleet of quadrotor micro aerial vehicles (MAVs) operating in uncertainty and susceptible to disturbance environments. The key innovation lies in a single-gain adaptive sliding mode control (SGASMC) strategy that guarantees practical finite-time convergence in the presence of external disturbances—modeled using the Von Kármán turbulence model—and system uncertainties. Unlike traditional approaches, the proposed method enables follower agents to track a dynamically evolving convex hull defined by leader agents with unknown control inputs, while also ensuring real-time sensor-less inter-agent collision avoidance and trajectory tracking within confined, time-varying environments.

The controller adaptively estimates and minimizes control gains. This approach avoids overestimation, thereby improving control efficiency and responsiveness. A Lyapunov-based stability analysis confirms finite-time convergence and robustness. Simulation results incorporating the full nonlinear quadrotor dynamics of the quadrotor to validate the framework's effectiveness. The system achieves robust containment, integrated collision avoidance, and accurate trajectory tracking under realistic aerodynamic disturbances.

The proposed method offers a scalable and adaptable control solution for real-world MAV applications, particularly in dynamic and uncertain indoor environments.

The rest of this work is organized as follows: Section 2 covers preliminary concepts and the problem formulation. Section 3 presents the proposed formation-containment controller and the stability analysis. Simulation results are presented in Section 4. Finally, in Section 5, conclusions are drawn.

2. Preliminaries and Problem Statement

This section covers the fundamental principles of graph theory required to establish an interaction network for the quadrotor fleet and introduces the concept of the Hadamard product. Additionally, the paper presents the problem formulation.

2.1. Graph Theory

For an easy representation of the interaction between the quadrotor fleet, this paper uses graph theory. The essential concepts of graph theory are presented in the following paragraphs. The system consists of n followers and m leaders. Let a graph $\mathcal{G}(V, \varepsilon)$ represents the directed flow of information among elements of the system. $V = \{v_1, \dots, v_{n+m}\}$ is a set of nodes that represent the elements, and $\varepsilon(i, j) \subseteq V \times V \in \mathcal{R}$ is the edge set for the interactions. The interactions of the system can be represented by an adjacency matrix $A = [a_{ij}]$, where $a_{ij} = 1 \forall i \neq j$ if there is an edge connecting nodes v_i and v_j , and $a_{ij} = 0$ otherwise. Denote a diagonal degree matrix $D = \text{diag}(d_1, d_2, \dots, d_{n+m})$, where $d_{ii} = \sum_{j=1}^{n+m} a_{ij}$. A Laplacian Matrix $L = [l_{ij}]$ associated with \mathcal{G} is obtained by $L = D - A$. In the formation-containment context, we assume that leaders send only position information to their connected followers but do not receive any information from them, and the follow-

ers can send and receive information from the elements connected to them. Consequently, it is possible to divide the Laplacian matrix as follows:

$$L = \begin{bmatrix} L_N & L_M \\ 0_{m \times n} & 0_{m \times m} \end{bmatrix}$$

where $L_N \in \Re^{n \times n}$ and $L_M \in \Re^{n \times m}$ denote submatrices that represent the interactions follower-to-follower and leader-to-follower, respectively.

Assumption 1. For any follower agent on the graph \mathcal{G} , there exists a directed path such that it can receive information from at least one leader agent.

Under Assumption 1

- All the eigenvalues of L_N are positive, as it is a positive-definite Hermitian matrix.
- For matrix multiplication $-L_N^{-1}L_M$, the sum of each row is equal to 1, and all its elements are non-negative.

2.2. Hadamard Product

Hadamard product \odot or element-wise product is a matrix product of two matrices of the same dimension. For two matrices A and B , of the same dimension $m \times n$, the Hadamard product is defined as $(A \odot B)_{ij} = (A)_{ij}(B)_{ij}$. Any vector x can be expressed as its corresponding diagonal matrix D_x that has x as the main diagonal. The Hadamard product of two vectors x and y equals the matrix multiplication of the corresponding diagonal matrix of one of the vectors by the other vector: $x \odot y = D_x y = D_y x$. This allows the use of roots $D_{x^{1/2}}$, powers D_{x^2} , and performs other useful functions, such as the absolute value $D_{|x|}$.

2.3. Problem Formulation

Consider a quadrotor fleet consisting of $n + m$ agents, where n are followers, and m are leaders. Each agent is modeled as

$$\ddot{\chi}_i = f(\chi_i, t) + g(\chi_i)U_i + \Delta_i(t), \quad (1)$$

with $\chi \in \Re^n$ denoting the state, U is the controller and Δ represents perturbations/uncertainties. The formation-containment requires that every follower i adheres to a position inside of a convex hull generated by the leaders j . This formation is coordinated using the reference position of a virtual leader.

The control objective is to develop a robust formation and collision-free containment control for each agent to achieve the following tasks:

1. Trajectory tracking. To drive the state of each leader agent χ_j , with $j = n + 1, \dots, n + m$, to move along a desired trajectory such that

$$\|\chi_j - \chi_{jd}\| \rightarrow 0, \quad (2)$$

in finite time, where χ_{jd} is a desired position relative to a virtual leader χ_0 .

2. Coordinated containment. To ensure that the state of each follower agent χ_i , with $i = 1, \dots, n$, moves towards a desired position χ_{id} that lies inside of a convex hull defined according to the leader's position, ensuring

$$\|\chi_i - \chi_{id}\| \rightarrow 0, \quad (3)$$

in finite time. These convex hulls are defined as

$$Co(\chi_h) = \left\{ \sum_{j=n+1}^{n+m} a_j \chi_j \Leftrightarrow a_j \geq 0, \sum_{j=n+1}^{n+m} a_j = 1 \right\} \quad (4)$$

and

$$Co(\dot{\chi}_h) = \left\{ \sum_{j=n+1}^{n+m} b_j \dot{\chi}_j \Leftrightarrow b_j \geq 0, \sum_{j=n+1}^{n+m} b_j = 1 \right\} \quad (5)$$

where the positions and velocities of the n followers are constrained by the states χ_j of the m leaders. a and b represent scalar sets defining a convex linear combination for position and velocity. Therefore, such a convex hull represents the linear combination of the states of the leaders.

3. Containment Collision avoidance. To control the state of each agent χ_k , with $k = 1, \dots, n + m$, to avoid other agents in the system such that

$$\|\chi_k - \chi_n\| \geq \gamma_s \quad (6)$$

where $n \neq k$ and γ_s is a defined safety distance relative to the other agents.

3. Formation Collision-Free Containment Control Design

In this section, the design of the proposed formation and collision-free containment controller is described, where control law designs were based on a class of adaptive sliding mode controllers. This implementation employs a two-layer strategy. Initially, the leaders track a desired trajectory using a virtual leader as a reference. Then, the followers converge within the convex hull formed by the leaders. Figure 1 presents the interactions among followers, leaders, and a virtual leader.

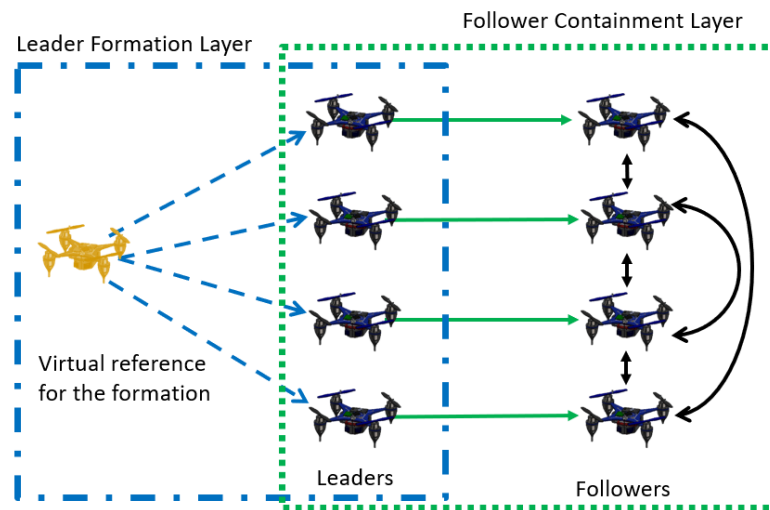


Figure 1. Two-layer structure and interaction network of the quadrotor fleet.

The system considers a virtual leader. Using its position as a reference for the formation of the leader subgroup, the reference state is defined as

$$\chi_0 = [x_0, \dot{x}_0, y_0, \dot{y}_0, z_0, \dot{z}_0]^T \quad (7)$$

We denote a formation matrix $h = [h_{n+1}^T, h_{n+2}^T, \dots, h_{n+m}^T]^T$ within $h_j = [h_{p,j}, h_{v,j}] \in \mathbb{R}^6, \forall j = n+1, n+2, \dots, n+m$, describing the desired formation of the leaders. Since this work evaluates the problem of time-varying formations, let us define the following assumption.

Assumption 2. The formation vectors h_j for all $j = n+1, n+2, \dots, n+m$ are piecewise continuously differentiable.

To achieve formation tracking, for all leaders with any initial conditions, the system should satisfy the following:

$$\lim_{t \rightarrow \infty} (\chi_j - h_j - \chi_0) = 0, \forall j = n+1, n+2, \dots, n+m \quad (8)$$

As such, desired formation positions are defined as $\chi_{d,j} = \chi_0 + h_j \forall j = n+1, n+2, \dots, n+m$. Thus, a tracking error is established as

$$e_t = \chi_{1,0} + h_{p_j} - \chi_{1,j}, \quad \dot{e}_t = \chi_{2,0} + h_{v_j} - \chi_{2,j}, \quad (9)$$

Then, to lay the foundation of containment, the following assumption is stated:

Assumption 3. The complete state of MAVs is assumed to be available to its neighbors.

This study focuses on the control strategy to ensure collision-free containment of a MAV fleet, integrating the dynamics of each follower and the corresponding containment control law. To establish formation and collision-free containment, considering the flight capabilities of the quadrotors, such as their ability to vertically take-off and land, hover, and perform high-maneuverability maneuvers within a 3D workspace, it is assumed that each agent is equipped with a low-level controller enabling free maneuverability. A reduced tracking model is used to determine the desired positions for formation and containment with respect to the inertial frame I [29]:

$$\ddot{x} = a_x \cos \psi - a_y \sin \psi - \dot{\psi}(v_x \sin \psi + v_y \cos \psi) \quad (10)$$

$$\ddot{y} = a_x \sin \psi + a_y \cos \psi + \dot{\psi}(v_x \cos \psi - v_y \sin \psi) \quad (11)$$

$$\ddot{z} = a_z \quad (12)$$

$$\ddot{\psi} = \Omega \quad (13)$$

with accelerations a_x, a_y, a_z in x, y, z coordinates, while v_x and v_y denote velocities with respect to the body frame $\{\mathbf{B}_i\}$ and Ω is the angular acceleration in yaw.

From the model (10)–(13), and considering a vector state as $\xi = [x, y, z, \psi]^T$ of each agent, the system is rewritten as follows:

$$\ddot{\xi}_i = F(\xi_i, t) + g(\xi_i)U_i + \Delta_i(t), \quad (14)$$

with

$$F(\xi_i, t) = \begin{bmatrix} -\dot{\psi}_i(\dot{x}_i \sin \psi_i + \dot{y}_i \cos \psi_i) \\ \dot{\psi}_i(\dot{x}_i \cos \psi_i - \dot{y}_i \sin \psi_i) \\ 0 \\ 0 \end{bmatrix},$$

$$g(\xi_i) = \begin{bmatrix} \cos \psi_i & -\sin \psi_i & 0 & 0 \\ \sin \psi_i & \cos \psi_i & 0 & 0 \\ 0 & 0 & 1 & 0 \\ 0 & 0 & 0 & 1 \end{bmatrix}, \quad (15)$$

where $U_i = [a_x, a_y, a_z, \alpha]^T$ is the control command. The perturbations and uncertainties are represented by $\Delta_i(t) = [\delta_x, \delta_y, \delta_z, \delta_\omega]^T$ satisfying $|\Delta_i(t)| \leq L$, with $L > 0$ denoting the

perturbation boundary. Now, based on Assumption 1, to satisfy coordinated containment, the positions and velocities desired for the i -th follower are defined as follows:

$$\xi_{dci} = \sum_{j=1}^m [-L_N^{-1} L_M]_{ij} \xi_{n+j} = [x_{dci} \quad y_{dci} \quad z_{dci} \quad \psi_{dci}]^T \quad (16)$$

$$\dot{\xi}_{dci} = \sum_{j=1}^m [-L_N^{-1} L_M]_{ij} \dot{\xi}_{n+j} = [\dot{x}_{dci} \quad \dot{y}_{dci} \quad \dot{z}_{dci} \quad \dot{\psi}_{dci}]^T \quad (17)$$

where ξ_{n+j} and $\dot{\xi}_{n+j}$ are the leader $(n + j)$ -th states. Subsequently, the containment error is formulated as

$$e_c = \xi_{dci} - \xi_i = \sum_{j=1}^m [-L_N^{-1} L_M]_{ij} \xi_{n+j} - \xi_i, \quad (18)$$

and their derivative corresponds to

$$\dot{e}_c = \dot{\xi}_{dci} - \dot{\xi}_i = \sum_{j=1}^m [-L_N^{-1} L_M]_{ij} \dot{\xi}_{n+j} - \dot{\xi}_i, \quad (19)$$

See Figure 2.

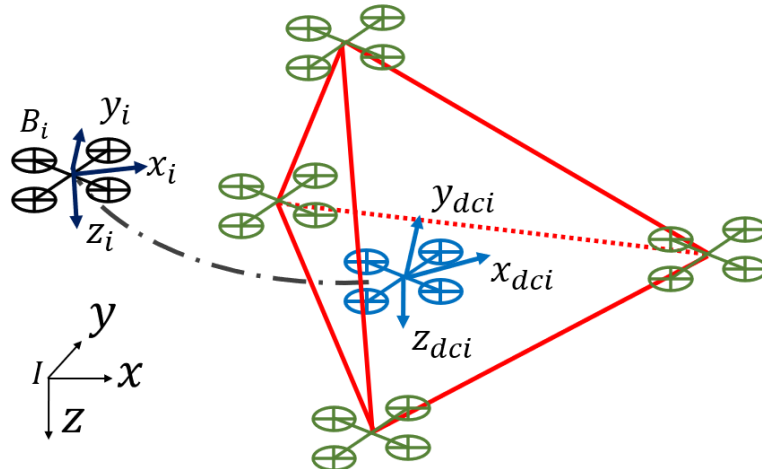


Figure 2. Tracking model for each follower.

Now, since the containment error is calculated individually for each follower based on the current positions of the leaders, the actual trajectories of the followers to reach the desired position may generate collisions during the convergence phase. Thus, to guarantee collision-free convergence for the followers, the following strategy is adopted:

$$e_{aci} = e_ci + h_ci \quad (20)$$

where the error is expanded by the desired distance relative to all neighbor agents h_ci , this adds a repelling effect, making agents pursue their desired positions while maintaining proportional distances from each other, thus assuring (6). Using the same information as that for the containment error, we construct h_ci . To simplify computation, the containment error is expressed as matrix multiplication:

$$e_ci = (L_\xi \otimes I_s) \xi - (I_{n+m} \otimes I_s) \xi \quad (21)$$

$$L_\zeta = \begin{bmatrix} 0 & -L_N^{-1} L_M \\ 0 & I_m \end{bmatrix} \quad (22)$$

where ξ describes the states of all agents in the system, I_* is an identity matrix whose size is $*$, and s is the number of states of each agent. The desired distance relative to the neighbors is given by

$$h_c i = \{(D \otimes I_s)(L_\zeta \otimes I_s)\xi - (A \otimes I_s)(L_\zeta \otimes I_s)\xi\} - (L \otimes I_s)\xi \quad (23)$$

By substituting Equations (21) and (23) into (20), we obtain the following:

$$\begin{aligned} e_{ac} i &= (L_\zeta - I_{n+m}) \otimes I_s \xi + (DL_\zeta - AL_\zeta - L) \otimes I_s \xi \\ &= (L_\zeta - I_{n+m} + (D - A)L_\zeta - L) \otimes I_s \xi \\ &= (L_\zeta - I_{n+m} + LL_\zeta - L) \otimes I_s \xi \\ &= (L_\zeta - I_{n+m} - L) \otimes I_s \xi \end{aligned} \quad (24)$$

Due to the fact that $(L_\zeta - I_{n+m} - L) \otimes I_s$ is a constant matrix and judging by the properties established in the Assumption 1, we know that all its eigenvalues are non-positive. Now, the error time derivative result is as follows:

$$\dot{e}_{ac} i = (L_\zeta - I_{n+m} - L) \otimes I_s \dot{\xi} \quad (25)$$

Then, to design the formation and collision-free containment control, using the SGASMC strategy, a containment sliding surface is denoted as:

$$\sigma_c = \dot{e}_{ac} + D_\lambda e_{ac} \quad (26)$$

where D_λ is the diagonal matrix representation of the vector λ such that $\lambda_i > 0 \ \forall i$ and the time derivative of (26) is given by

$$\begin{aligned} \dot{\sigma}_c &= \ddot{e} + D_\lambda \dot{e} \\ &= -(F_i(\dot{\xi}_i, \xi_i) + g(\xi_i)U + \Delta(t)) + D_\lambda \dot{e} \end{aligned} \quad (27)$$

The control aims to achieve $\sigma = \dot{\sigma} = 0$. Thus, the next feedback control is adopted:

$$U_i = g(\xi_i)^{-1}(-F_i(\dot{\xi}_i, \xi_i) - u_i(t) + D_\lambda e_c), \quad (28)$$

where the auxiliary controller u_i is applied using a single-gain adaptive sliding mode strategy, as detailed in

$$u_i = -2K_c(t)|\sigma_c|^{1/2} sign(\sigma_c) - \frac{K_c^2}{2}\sigma_c, \quad (29)$$

whose adaptation of $K_c(t)$ is governed by

$$\dot{K}_c(t) = \alpha_c^{1/2}|\sigma|^{1/2} - \beta_c^{1/2}K_c(t)^2 \quad (30)$$

with α_c and β_c being positive and representing the precision and control effort parameters, respectively. β_c is usually a small value as it helps minimize oscillation and smooth the control action. α_c is generally larger, controlling the rate at which the adaptive gain grows; however, as its value increases, the adaptation becomes more aggressive, leading to higher energy consumption. The advantages of the proposed controller (29) and adaptation (30)

include robustness against external disturbances, avoidance of overestimation of controller gains, reduction in control parameters and achieving finite-time convergence.

Stability Analysis

The stability of the formation-containment closed-loop system is presented. Let us first consider the following definition and lemma, respectively.

Definition 1 ([30]). *Considering a nonlinear system*

$$\dot{\xi} = f(\xi, U) \quad (31)$$

where ξ is a state vector, U is the input vector. The solution is practical finite-time stable if for all ξ_0 there exists a $\epsilon > 0$ and a time $t_c(\epsilon, \xi_0) < \infty$, such that $\|\xi(t)\| < \epsilon$, for all $t \geq t_0 + t_c$.

Lemma 1 ([30]). *Consider a nonlinear system (31), and assume there exists a continuous positive-definite function $V(\sigma)$ and scalars $\eta > 0$, $0 < \alpha < 1$ and $0 < \varsigma < \infty$ such that*

$$\dot{V}(\sigma) \leq \eta V^\alpha(\sigma) + \varsigma, \quad (32)$$

the system is practical finite-time stable. Therefore, the trajectories of the closed-loop system are bounded in finite time as

$$\lim_{\vartheta \rightarrow \vartheta_0} \sigma \in \left(V^\alpha(\sigma) \leq \frac{\varsigma}{(1 - \vartheta)\eta} \right) \quad (33)$$

where $0 < \vartheta_0 < 1$. Therefore, the trajectories of the closed-loop system are bounded in finite time by

$$t_c \leq \frac{V^{1-\alpha}(\sigma_0)}{\eta \vartheta_0 (1 - \alpha)} \quad (34)$$

Now, the stability of the system can be expressed by the following theorem.

Theorem 1. *A system considering the formation-containment controller (28) with adaptive law (30) in a closed-loop with a 3D tracking model (10)–(13) for a mini quadrotor fleet is practical finite-time stable and converges at time $t \leq t_c$.*

Proof. The closed-loop stability can be assessed by examining the dynamics of the formation-containment sliding surface when integrated with the controller (28), which is expressed by

$$\begin{aligned} \dot{\sigma}_c &= -(F_i(\dot{\xi}_i, \xi_i) + g_i(\xi_i)(g_i(\xi_i)^{-1}(-F_i(\dot{\xi}_i, \xi_i) - u_i(t) + D_\lambda \dot{e}) + \Delta(t)) + D_\lambda \dot{e}) \\ &= u_i(t) - \Delta(t) \\ &= -2K_c |\sigma_c|^{1/2} sign(\sigma_c) - \frac{K_c^2}{2} \sigma_c + \Delta(t) \end{aligned} \quad (35)$$

To simplify the analysis, and since $K_c(t)$ is a diagonal matrix, each of its values individually affects only one of the states of the system; it is possible to continue the closed-loop stability analysis as follows:

$$\dot{\sigma}_c = -2K_c |\sigma_c|^{1/2} D_{sign(\sigma_c)} - \frac{K_c^2}{2} \sigma_c + D_{\delta(t)} \quad (36)$$

Now, consider the following Lyapunov function candidate:

$$V = \frac{1}{2} \sigma_c^T \sigma_c + \frac{1}{2} (K_c - K_c^*)^T (K_c - K_c^*) \quad (37)$$

where K_c^* is a gain upper-bound, which exists but is unknown, and counteracts the perturbation, such that $\Delta K_c = K_c - K_c^* < 0$. Then, by differentiating such a Lyapunov function candidate, we have

$$\dot{V} = \sigma_c^T \dot{\sigma}_c + \Delta K_c^T \dot{K}_c \quad (38)$$

where introducing (36) into (37) leads to

$$\dot{V} \leq \sigma_c^T (-2K_c|\sigma_c|^{1/2} D_{\text{sign}(\sigma_c)} - \frac{K_c^2}{2}\sigma_c + D_{\delta(t)}) + \Delta K_c^T \dot{K}_c \quad (39)$$

$$\leq |\sigma_c|^T (-2K_c|\sigma_c|^{1/2} - \frac{K_c^2}{2}|\sigma_c| + L) + \Delta K_c^T \dot{K}_c \quad (40)$$

Given this includes only dot products and Hadamard products, it can be rewritten as

$$\dot{V} \leq \sum_{i=1}^{n+m} \{ |\sigma_{ci}| (-2K_{ci}|\sigma_{ci}|^{1/2} - \frac{K_{ci}^2}{2}|\sigma_{ci}| + L_i) + \Delta K_{ci} \dot{K}_{ci} \} \quad (41)$$

$$\leq \sum_{i=1}^{n+m} \{ -2K_{ci}|\sigma_{ci}|^{3/2} - \frac{K_{ci}^2}{2}|\sigma_{ci}|^2 + L_i|\sigma_{ci}| + \Delta K_{ci} \dot{K}_{ci} - 2K_c^*|\sigma_c|^{3/2} + 2K_c^*|\sigma_c|^{3/2} \} \quad (42)$$

$$\leq \sum_{i=1}^{n+m} \{ |\sigma_{ci}| (-2K_{ci}^*|\sigma_{ci}|^{1/2} - \frac{K_{ci}^2}{2}|\sigma_{ci}| + L_i) + \Delta K_{ci} (\dot{K}_{ci} - 2|\sigma_{ci}|^{3/2}) \} \quad (43)$$

$$\leq |\sigma_c|^T (-2K_c^*|\sigma_c|^{1/2} - \frac{K_c^2}{2}|\sigma_c| + L) + \Delta K_c^T (\dot{K}_c - 2|\sigma_c|^{3/2}) \quad (44)$$

Now, by introducing the following parameters and knowing that $\Delta K_c = -|\Delta K_c|$

$$\eta_k \geq 0 \quad (45)$$

$$\eta_s = 2K_c^*|\sigma_c|^{1/2} + \frac{K_c^2}{2}|\sigma_c| - L, \quad (46)$$

one can express the above equation as

$$\dot{V} \leq -\eta_s^T |\sigma_c| - \eta_k^T |\Delta K_c| + \eta_k^T |\Delta K_c| + \Delta K_c^T (\dot{K}_c - 2|\sigma_c|^{3/2}) \quad (47)$$

$$\leq -\eta_s^T |\sigma_c| - \eta_k^T |\Delta K_c| + |\Delta K_c|^T (-\dot{K}_c + 2|\sigma_c|^{3/2} + \eta_k) \quad (48)$$

Consider

$$\eta_s^T |\sigma_c| = \sum_{i=1}^{n+m} (\eta_s)_i |\sigma_{ci}| = \sum_{i=1}^{n+m} |\sigma_{ci}|^{1/2} (\eta_s)_i |\sigma_{ci}|^{1/2} = (|\sigma_c|^{1/2})^T D_{\eta_s} |\sigma_c|^{1/2} \quad (49)$$

and let $\zeta = |\Delta K_c|^T (-\dot{K}_c + 2|\sigma_c|^{3/2} + \eta_k) = |K_c - K_c^*|(-\alpha_c^{1/2}|\sigma_c|^{1/2} + \beta_c^{1/2}K_c^2 + |\sigma_c|^{3/2} + \eta_k)$, then

$$\dot{V} \leq -(|\sigma_c|^{1/2})^T D_{\eta_s} |\sigma_c|^{1/2} - (|\Delta K_c|^{1/2})^T D_{\eta_k} |\Delta K_c|^{1/2} + \zeta \quad (50)$$

From the definition of η_s and η_k , it is possible to conclude that D_{η_s} and D_{η_k} are positive-definite symmetric matrices. Thus, by Rayleigh's principle,

$$\begin{aligned} -(|\sigma_c|^{1/2})^T D_{\eta_s} |\sigma_c|^{1/2} &\leq -\lambda_{\min}(D_{\eta_s}) (|\sigma_c|^{1/2})^T |\sigma_c|^{1/2} \\ &\leq -\lambda_{\min}(D_{\eta_s}) \sum_{i=1}^{n+m} |\sigma_{ci}| \\ -(|\Delta K_c|^{1/2})^T D_{\eta_k} |\Delta K_c|^{1/2} &\leq -\lambda_{\min}(D_{\eta_k}) \sum_{i=1}^{n+m} |K_{ci} - K_{ci}^*| \end{aligned}$$

where $\lambda_{\min}(\cdot)$ is the minimum eigenvalue of \cdot . Then,

$$\dot{V} \leq -\lambda_{\min}(D_{\eta_s}) \sum_{i=1}^{n+m} \{|\sigma_{ci}|\} - \lambda_{\min}(D_{\eta_k}) \sum_{i=1}^{n+m} \{|K_{ci} - K_{ci}^*|\} + \varsigma \quad (51)$$

$$\leq -\lambda_{\min}(D_{\eta_s}) \sqrt{2} \sum_{i=1}^{n+m} \left\{ \frac{|\sigma_{ci}|}{\sqrt{2}} \right\} - \lambda_{\min}(D_{\eta_k}) \sqrt{2} \sum_{i=1}^{n+m} \left\{ \frac{|K_{ci} - K_{ci}^*|}{\sqrt{2}} \right\} + \varsigma \quad (52)$$

$$\leq \eta \left[\sum_{i=1}^{n+m} \left\{ \frac{|\sigma_{ci}|}{\sqrt{2}} + \frac{|K_{ci} - K_{ci}^*|}{\sqrt{2}} \right\} \right] + \varsigma \quad (53)$$

$$\leq \eta \left(\frac{|\sigma_c|}{\sqrt{2}} + \frac{|K_c - K_c^*|}{\sqrt{2}} \right) + \varsigma \quad (54)$$

with $\eta = \min\{\sqrt{2}\lambda_{\min}(D_{\eta_s}), \sqrt{2}\lambda_{\min}(D_{\eta_k})\}$. The above equation can be rewritten according to Lemma 1, resulting in the following:

$$\dot{V} \leq \eta V^\alpha + \varsigma, \quad (55)$$

where $\alpha = 1/2$. Thus, σ is practical finite-time stable if $0 < \varsigma < \infty$. Notice that ς must be positive to guarantee stability; in that way, two cases arise:

- Case 1. When the sliding mode is achieved, i.e., $|\sigma| = 0$ and $\varsigma > 0$ if $\beta_c^{1/2} K_c^2 + \eta_k > 0$ due to the fact that β_c , and K_c are positive defined, then $\varsigma > 0 \forall \eta_k > 0$.
- Case 2. For the reaching phase $|\sigma| \neq 0$ and $\varsigma > 0$ if $-\alpha_c^{1/2} |\sigma|^{1/2} + \beta_c^{1/2} k^2 + 2|\sigma|^{3/2} + \eta_k > 0$, one can choose $\eta_k = (\alpha_c^{1/2} (\alpha_c^{1/2}/6)^{1/2} - 2(\alpha_c^{1/2}/6)^{3/2})$ to allow $\varsigma > 0$.

This completes the proof. \square

For low-level control and modeling, the results from [31] guided the development of a control strategy for a six-degree-of-freedom quadrotor model, which reflects the cross configuration and uses these parameters: $l = 0.058$ m, $g = 9.81$ m/s², $m = 0.060$ kg, $I_{xx} = 3.073 \times 10^{-5}$ kgm², $I_{yy} = 3.084 \times 10^{-5}$ kgm², $I_{zz} = 5.968 \times 10^{-5}$ kgm², $J_r = 8.801 \times 10^{-8}$ kgm². The flight controller is divided into two parts: an attitude controller for the ϕ, θ, ψ angles in the body frame, and a position controller for the x, y, z coordinates in the inertial frame. The controllers are implemented as presented in [29]. This approach enables the calculation of the torques, thrusts, and desired angles required for free maneuverability in a 3D workspace.

4. Simulation Results

This section presents the evaluation of the proposed three-dimensional formation-containment control strategy for a fleet of quadrotor micro aerial vehicles. The simulation was implemented in the MATLAB/Simulink R2020b environment, incorporating both the control algorithm and a dynamic quadrotor model for each agent. Figure 3 illustrates the control loop that integrates the two control layers. The proposed SGASMC controls the tracking model to set the trajectory of each agent, and low-level attitude and position control ensures maneuverability. The simulated system consists of eight agents: four followers, denoted as F_1-F_4 , and four leaders, as L_1-L_4 . The interactions among the agents are depicted in Figure 1.

Simulations were conducted using a fixed step size of 0.01 s. To demonstrate the effectiveness of the proposed approach, the test trajectory was designed to represent several common scenarios in multi-agent systems missions, including static and dynamic convergence, robustness to perturbations, and time-varying formations.

The Von Kármán turbulence model is used to simulate atmospheric wind disturbances affecting unmanned aerial vehicles. It provides a realistic representation of wind turbulence

by modeling the power spectral density of velocity fluctuations based on assumptions of homogeneous turbulence. Compared to simpler models, this model more accurately captures the spatial and temporal characteristics of wind disturbances encountered by UAVs, making it suitable for high-fidelity simulation, flight dynamics analysis, and control system design. The dedicated block for Von Karman wind turbulence provided by Simulink was used in this simulation.

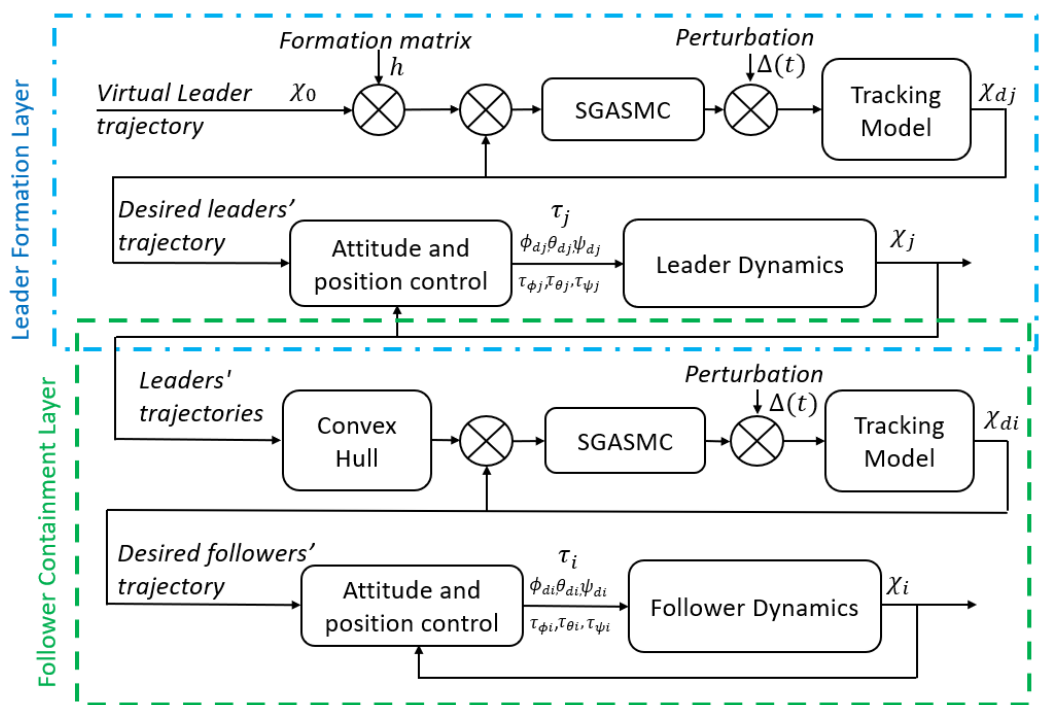


Figure 3. General control scheme: Leaders and followers.

The complete description of the test is presented in Figure 4. The initial conditions of the system are as follows: $F_1(0) = \xi_1(0) = [-0.7, 1, 0, 0]^T$, $F_2(0) = \xi_2(0) = [-2, 0, 0, 0]^T$, $F_3(0) = \xi_3(0) = [0.7, -1, 0, 0]^T$, $F_4(0) = \xi_4(0) = [1, 1, 0, 0]^T$, $L_1(0) = \xi_5(0) = [1, 0, 0, \pi]^T$, $L_2(0) = \xi_6(0) = [-1, 0, 0, \pi]^T$, $L_3(0) = \xi_7(0) = [0, 1, 0, \pi]^T$, $L_4(0) = \xi_8(0) = [0, -1, 0, \pi]^T$. All agents are considered to have the same characteristics, and as such, the control parameters are the same for each agent: $\alpha_i = 4$, $\beta_i = 0.125$, and $\lambda_i = 3$. The first phase involves followers converging to their designated reference point within a region defined by the leaders. During this phase, the leaders are arranged in a square formation, and the followers are expected to converge to the containment while avoiding collisions with both each other and the leaders. Once containment is achieved, the second phase commences. In this phase, the leaders follow a trajectory in the shape of a 3D infinity, as shown in Figures 5 and 6. Furthermore, to evaluate robustness, a turbulent wind perturbation using the Von Kármán model is applied starting at $t = 45$ s and for the remainder of the test. Its magnitude is presented in Figure 7. Under such perturbations, and given the quadrotor's small size, the disturbance magnitude presents a considerable challenge not only to maintain a stable flight but also to avoid collisions along the trajectory. At $t = 62.5$ s, the leaders' formation changes from a square to a tetrahedral shape. In this phase, followers pursue new desired positions that reflect the modification of the leader's formation, while maintaining the same interaction network. Finally, in the last phase, the system continues to follow the trajectory with the new formation and under the turbulent wind perturbation. A video of the simulation is attached to illustrate the system's dynamic response. This video (Video S1) visualizes results by importing simulation data for a full 6-degree of freedom quadrotor

model for each agent and disturbances using the Von Kármán wind turbulent model from MATLAB/Simulink into the CoppeliaSim Edu, Version 4.3.0 environment.

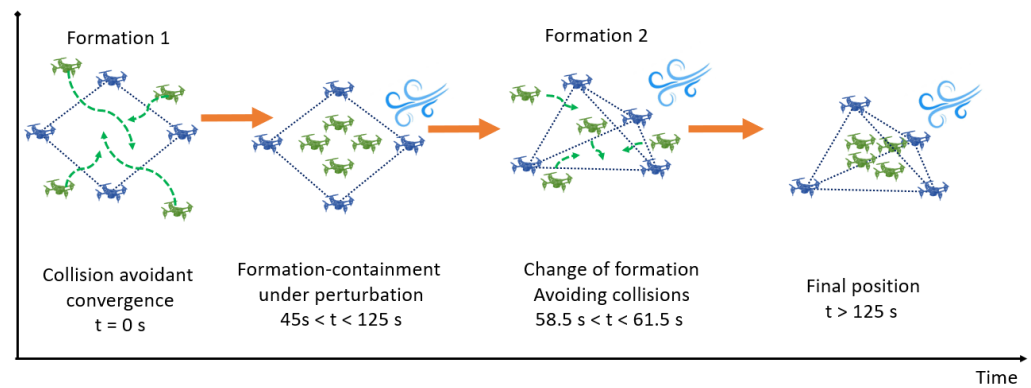


Figure 4. Description of the complete test.

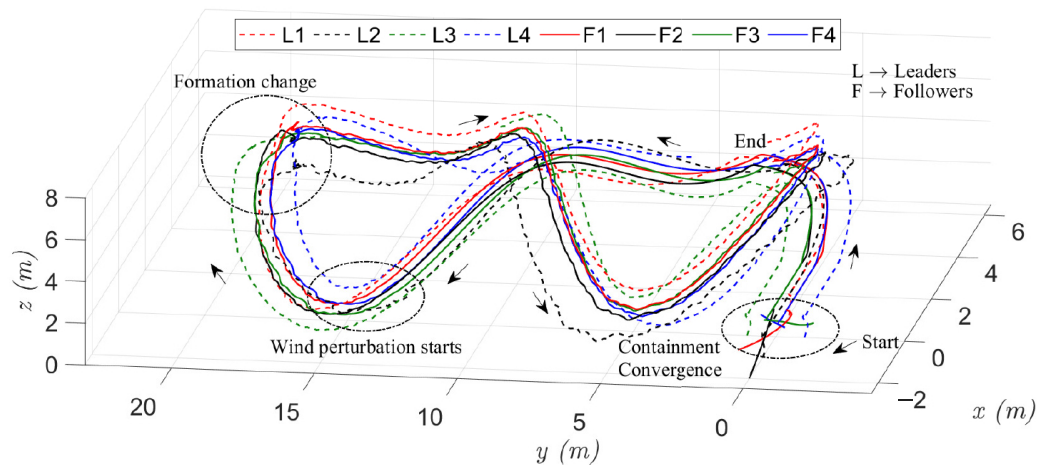


Figure 5. Quadrotors fleet response tracking a 3D trajectory.

To clarify the distinction between the normal containment error and the proposed collision avoidance error, Figures 8 and 9 display the convergence phase behaviors side by side for each control approach, using data from the first 5 s of the experiment. With the standard containment strategy, followers aim for their target positions by the shortest path. This can result in collisions, especially if the initial setup causes their paths to cross. For demonstration, the initial conditions were specifically chosen to create intersecting trajectories, illustrating how followers often reach their assigned altitude simultaneously and cross paths, which increases the risk of collision. In contrast, subsection (b) of the figures demonstrates the effects of the proposed collision avoidance error. Here, followers do not move directly to their desired positions. Instead, the control adjusts each follower's trajectory to avoid the expected desired positions of nearby agents. For example, follower F1 approaches its desired position from above, overshooting the required altitude before descending to it. F4, in turn, stays lower and follows a rising arc to join the formation from below. F2 and F3 show milder adjustments; F2 adds a slight curve to its path, giving F3 enough space to approach its position almost directly. This coordinated avoidance is achieved without relying on external sensors. Each follower maintains a safe distance using only the interaction network matrices and information shared by its neighbors. The followers' desired positions are determined by the submatrix $-L_N^{-1}L_M$ from L_ζ , which remains constant unless the network topology changes. As a result, any follower with access to the leaders' positions can calculate both its own and its neighbors' desired positions, enabling decentralized and collision-free convergence.

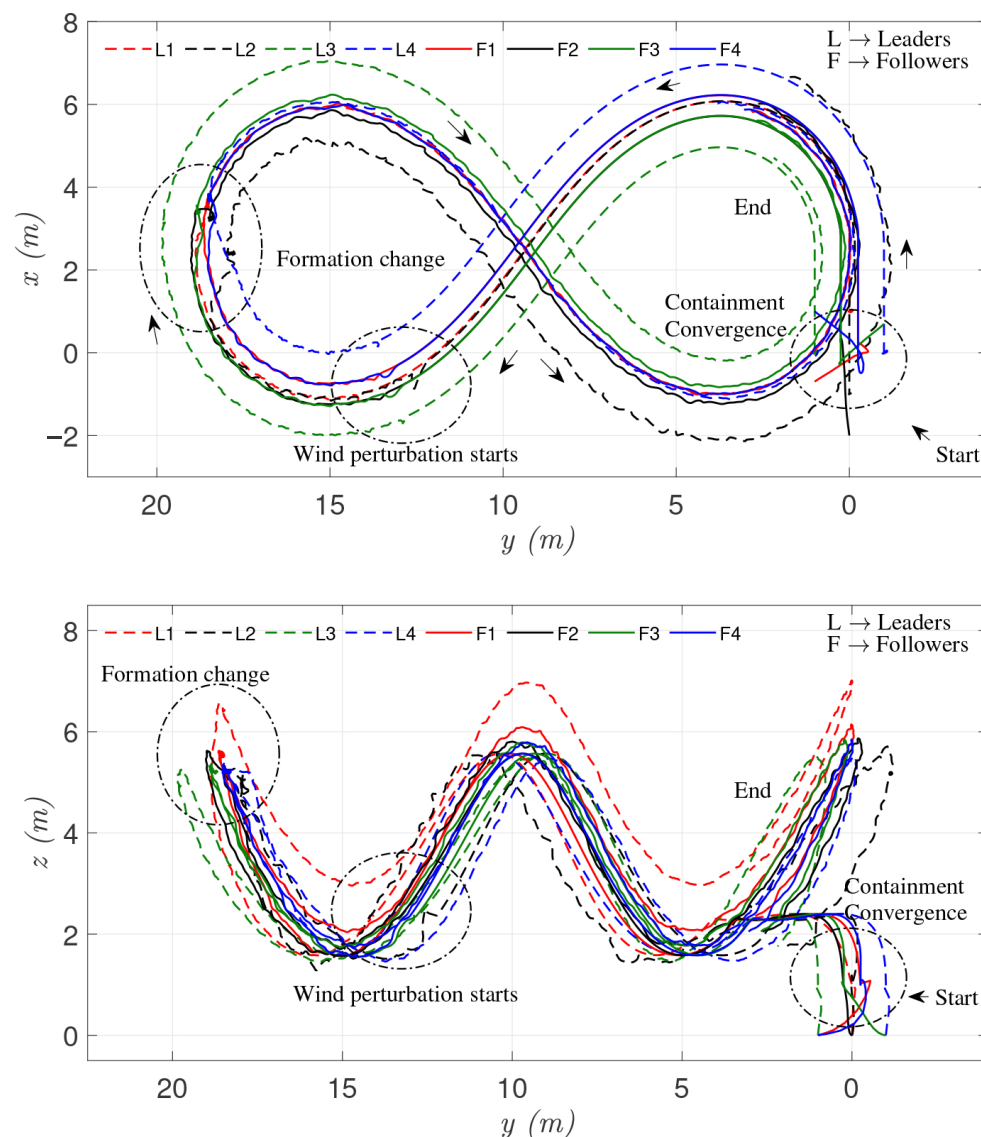


Figure 6. Top and front views of the fleet trajectories.

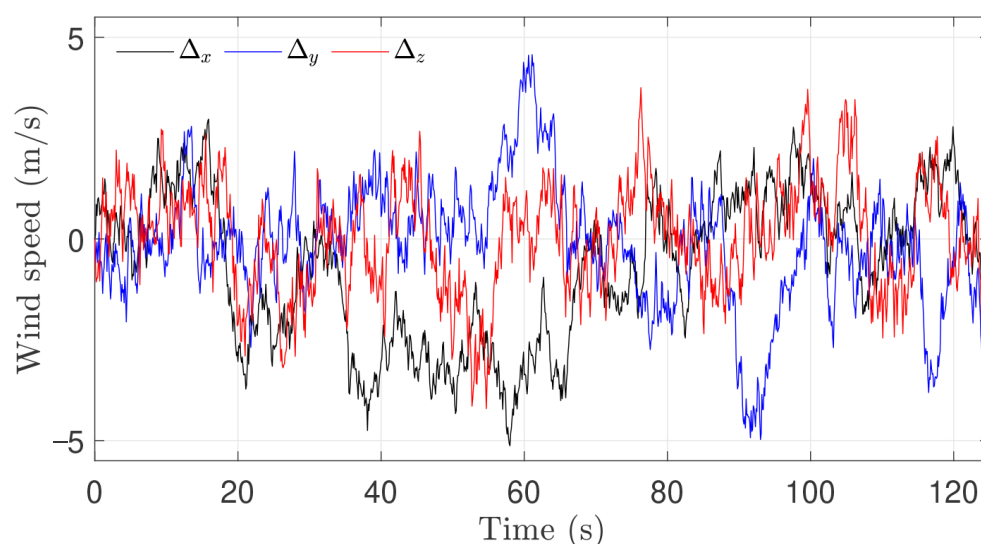


Figure 7. Applied wind perturbation profile.

Key system performance parameters are illustrated in the figures that follow. Figure 10 shows the norm of the position error and control input for the follower agents. The error represents the deviation between the actual follower positions and the desired positions defined by the convex hull formed by the leaders. This serves as an indicator of the containment performance, which is also illustrated in the lower panel of the figure, demonstrating that the magnitude of the control effort is within the capabilities of the MAVs. Figure 11 displays the evolution of the adaptive control gains for the followers under turbulent wind conditions. The variations in these gains reflect the controller's real-time adaptation to external disturbances, highlighting its ability to maintain stability and performance despite environmental perturbations. Figure 12 presents the tracking error norm for both followers and leaders. This error quantifies each agent's deviation from its respective reference trajectory, providing a measure of the overall system tracking performance. While the error exhibits spike increases, these are primarily due to the inertial effects inherent in the quadrotor dynamics. Importantly, these fluctuations remain within the allowable performance bounds of the vehicles. Notably, the leaders experience greater deviations than the followers under wind disturbances. This disparity occurs because the convex hull, which defines the formation, moves in response to leader displacement caused by disturbance. Conversely, the virtual leader, unaffected by atmospheric turbulence, continues along its predetermined trajectory, causing the leaders to exhibit a greater deviation from the ideal path under turbulent conditions.

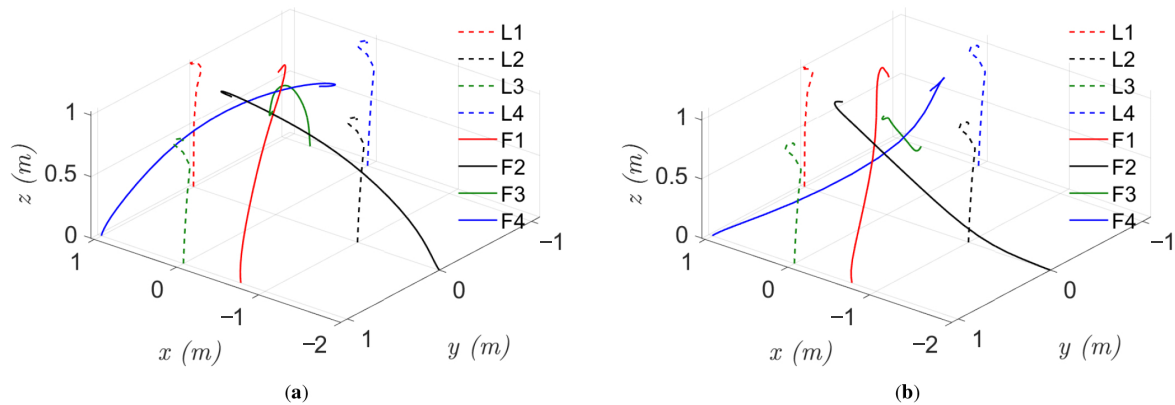


Figure 8. 3D view of convergence of all agents: (a) Followers collision during convergence; (b) Followers collision avoided during convergence.

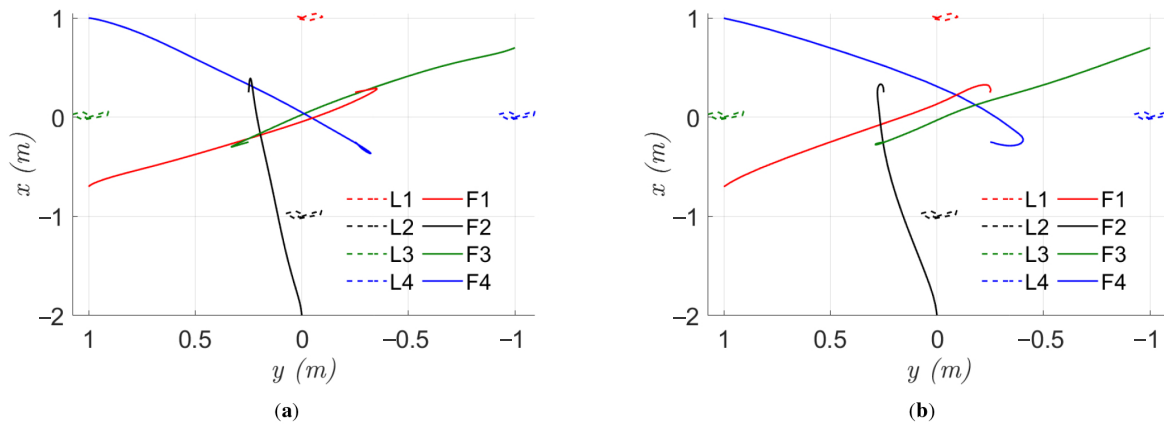


Figure 9. Top view of convergence of all agents: (a) Followers collision during convergence; (b) Followers collision avoided during convergence.

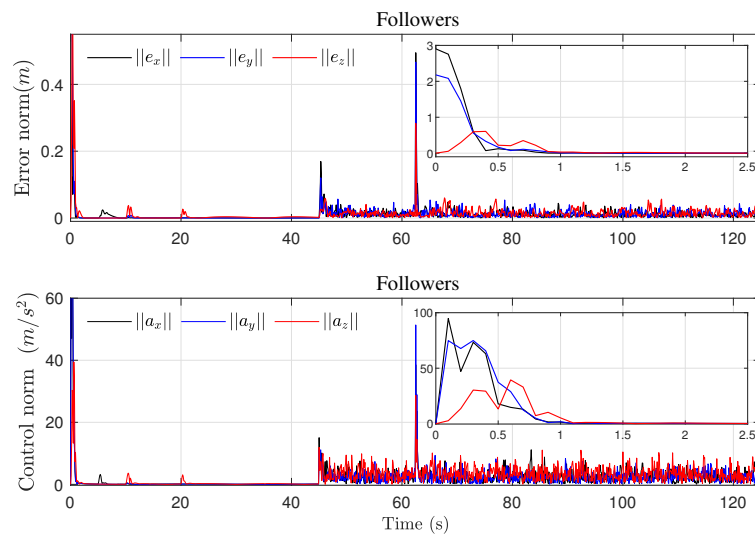


Figure 10. Containment error response (**top**) and containment control input norm (**bottom**), respectively.

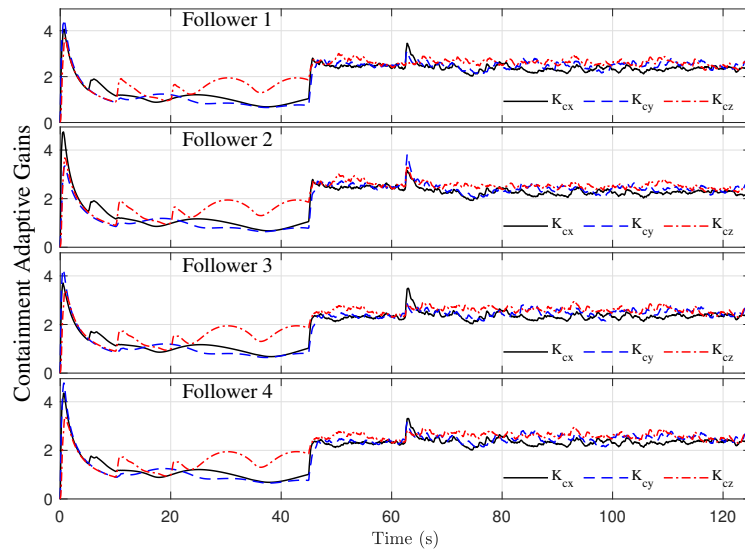


Figure 11. Adaptive gains of the containment scheme.

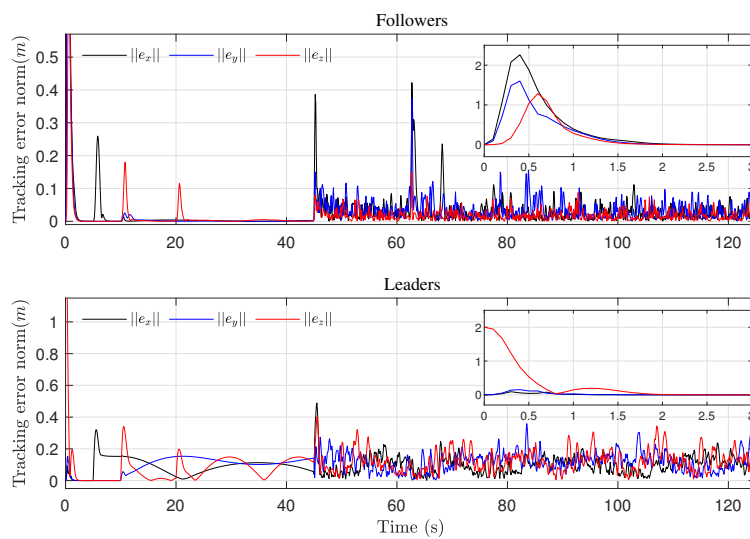


Figure 12. Tracking error of the formation-containment.

To further validate the effectiveness of the proposed controller, Figure 13 compares the performance of three control strategies in terms of the error norm, control effort norm, and integral absolute error (IAE) norm. All controllers were implemented within the same feedback linearization framework, with the control input u_i replaced by a conventional PID controller, an adaptive sliding mode controller (ASMC) [29], and the proposed SGASMC. As shown in the figure, all three controllers successfully maintained system stability under moderate Von Kármán wind disturbances. However, notable differences in performance are observed. The PID controller, lacking adaptive ability, exhibited greater difficulty in compensating for disturbances, resulting in higher error and control effort. In contrast, the two adaptive controllers, ASMC and SGASMC, demonstrated significantly better disturbance rejection, as reflected in their lower control effort norms. Among the adaptive strategies, the SGASMC exhibited a clear advantage in terms of adaptation speed. This is particularly evident in the IAE plot, where SGASMC shows a consistently lower growth rate, indicating faster convergence and more effective error suppression. These results highlight the superior performance of SGASMC in dynamic and uncertain environments compared to both ASMC and PID controllers.

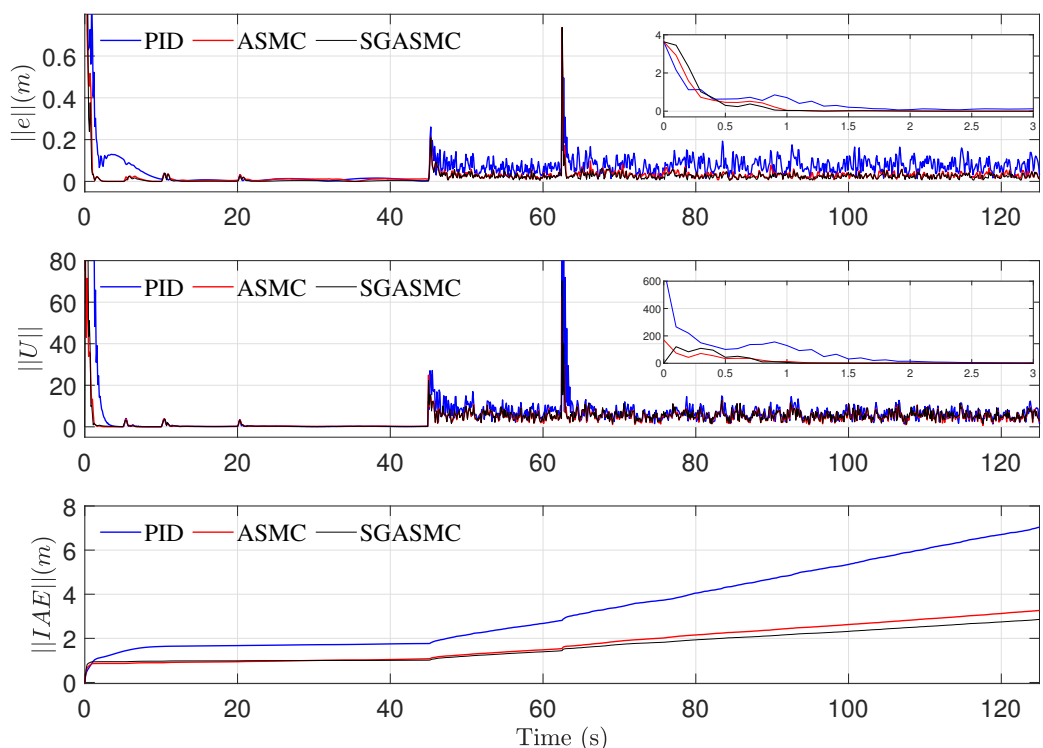


Figure 13. Comparison of the norm of the error, control, and integral absolute error for different controllers.

5. Conclusions

A formation and collision-free containment control strategy has been developed for a fleet of mini quadrotors. This control methodology was formulated using a class of adaptive sliding mode techniques, which ensures robustness against external disturbances and guarantees inter-agent collision avoidance during convergence. The control gain dynamically adapted its magnitude to counteract perturbations as they arose. Additionally, the practical finite-time stability of the system was proven using the Lyapunov approach. Simulation tests were conducted to assess the feasibility and performance of the proposed formation-containment strategy, using a realistic, complete quadrotor model and perturbations based on the Von Kármán turbulence model. The results demonstrated that the followers con-

verged to the convex hull while avoiding collisions, and the leaders successfully tracked a time-varying formation trajectory subjected to complex disturbances.

Supplementary Materials: The following supporting information can be downloaded at: <https://www.mdpi.com/article/10.3390/drones9100724/s1>.

Author Contributions: Conceptualization, C.K. and H.C.; methodology, C.K. and H.C.; software, C.K.; validation, H.C.; writing—original draft preparation, C.K.; writing—review and editing, C.K. and H.C. All authors have read and agreed to the published version of the manuscript.

Funding: This research received no external funding.

Data Availability Statement: The raw data supporting the conclusions of this article will be made available by the authors upon request.

Acknowledgments: Thanks are extended to the multi-robot system laboratory at Tecnológico de Monterrey and the CONACyT scholarship for support to develop this project.

Conflicts of Interest: The authors declare no conflicts of interest.

References

1. Feng, Z.; Hu, G.; Sun, Y.; Soon, J. An overview of collaborative robotic manipulation in multi-robot systems. *Annu. Rev. Control* **2020**, *49*, 113–127. <https://doi.org/10.1016/j.arcontrol.2020.02.002>.
2. Gupte, S.; Mohandas, P.; Conrad, J. A survey of quadrotor Unmanned Aerial Vehicles. In Proceedings of the 2012 Proceedings of IEEE Southeastcon, Orlando, FL, USA, 15–18 March 2012; pp. 1–6.
3. Kim, J.; Kim, S.; Ju, C.; Son, H.I. Unmanned Aerial Vehicles in Agriculture: A Review of Perspective of Platform, Control, and Applications. *IEEE Access* **2019**, *7*, 105100–105115. <https://doi.org/10.1109/ACCESS.2019.2932119>.
4. Beul, M.; Droeischel, D.; Nieuwenhuisen, M.; Quenzel, J.; Houben, S.; Behnke, S. Fast Autonomous Flight in Warehouses for Inventory Applications. *IEEE Robot. Autom. Lett.* **2018**, *3*, 3121–3128. <https://doi.org/10.1109/LRA.2018.2849833>.
5. Jadbbae, A.; Lin, J.; Morse, A. Coordination of groups of mobile autonomous agents using nearest neighbor rules. *IEEE Trans. Autom. Control* **2003**, *48*, 988–1001.
6. Ji, M.; Ferrari-Trecate, J.; Egerstedt, M.; Buffa, A. Containment control in mobile networks. *IEEE Trans. Autom. Control* **2008**, *53*, 1972–1975.
7. Meng, Z.; Ren, W.; Cao, Y.; You, Z. Leaderless and leader-following consensus with communication and input delays under a directed network topology. *IEEE Trans. Syst. Man Cybern. Part B Cybern.* **2011**, *41*, 75–88.
8. Meng, Y.; Chen, Q.; Chu, X.; Rahmani, A. Maneuver Guidance and Formation Maintenance for Control of Leaderless Space-Robot Teams. *IEEE Trans. Aerosp. Electron. Syst.* **2019**, *55*, 289–302. <https://doi.org/10.1109/TAES.2018.2850382>.
9. Ren, W. Distributed leaderless consensus algorithms for networked Euler-Lagrange systems. *Int. J. Control* **2009**, *82*, 2137–2149.
10. Ning, B.; Zuo, Z.; Jin, J.; Zheng, J. Distributed Fixed-Time Coordinated Tracking for Nonlinear Multi-Agent Systems Under Directed Graphs. *Asian J. Control* **2017**, *20*, 646–658. <https://doi.org/10.1002/asjc.1612>.
11. Parsa, M.; Danesh, M. Containment control of high-order multi-agent systems with heterogeneous uncertainties, dynamic leaders, and time delay. *Asian J. Control* **2019**, *23*, 799–810. <https://doi.org/10.1002/asjc.2251>.
12. Liu, Y.; Su, H. Some necessary and sufficient conditions for containment of second-order multi-agent systems with intermittent sampled data. *ISA Trans.* **2020**, *108*, 154–163. <https://doi.org/10.1016/j.isatra.2020.08.014>.
13. Wang, F.; Ni, Y.; Liu, Z.; Chen, Z. Containment Control for General Second-Order Multiagent Systems With Switched Dynamics. *IEEE Trans. Cybern.* **2020**, *50*, 550–560.
14. AL-Madani, B.; Elkhider, S.M.; El-Ferik, S. DDS-Based Containment Control of Multiple UAV Systems. *Appl. Sci.* **2020**, *10*, 4572. <https://doi.org/10.3390/app10134572>.
15. Wang, L.; Han, T.; Zhan, X.; Wu, J.; Yan, H. Bipartite containment for linear multi-agent systems subject to unknown exogenous disturbances. *Asian J. Control* **2021**, *24*, 1836–1845. <https://doi.org/10.1002/asjc.2580>.
16. Mazouchi, M.; Naghibi-Sistani, M.B.; Hosseini Sani, S.K.; Tatari, F.; Modares, H. Observer-based adaptive optimal output containment control problem of linear heterogeneous Multiagent systems with relative output measurements. *Int. J. Adapt. Control Signal Process.* **2019**, *33*, 262–284. <https://doi.org/10.1002/acs.2950>.
17. Amini, A.; Asif, A.; Mohammadi, A. Formation-containment control using dynamic event-triggering mechanism for multi-agent systems. *IEEE/CAA J. Autom. Sin.* **2020**, *7*, 1235–1248. <https://doi.org/10.1109/JAS.2020.1003288>.
18. Jiang, W.; Wen, G.; Peng, Z.; Huang, T.; Rahmani, A. Fully Distributed Formation-Containment Control of Heterogeneous Linear Multiagent Systems. *IEEE Trans. Autom. Control* **2019**, *64*, 3889–3896. <https://doi.org/10.1109/TAC.2018.2887409>.

19. Liu, D.; Liu, H.; Valavanis, K.P. Fully Distributed Time-Varying Formation Control for Multiple Uncertain Missiles. *IEEE Trans. Aerosp. Electron. Syst.* **2021**, *57*, 1646–1656. <https://doi.org/10.1109/TAES.2020.3046329>.
20. Fu, J.; Wan, Y.; Wen, G.; Huang, T. Distributed Robust Global Containment Control of Second-Order Multiagent Systems With Input Saturation. *IEEE Trans. Control Netw. Syst.* **2019**, *6*, 1426–1437.
21. Xiao, S.; Dong, J. Distributed Adaptive Fuzzy Fault-Tolerant Containment Control for Heterogeneous Nonlinear Multiagent Systems. *IEEE Trans. Syst. Man Cybern. Syst.* **2020**, *52*, 954–965.
22. Zhao, L.; Yu, J.; Shi, P. Command Filtered Backstepping-Based Attitude Containment Control for Spacecraft Formation. *IEEE Trans. Syst. Man Cybern. Syst.* **2021**, *51*, 1278–1287. <https://doi.org/10.1109/TSMC.2019.2896614>.
23. Kuang, J.; Chen, M. Adaptive Sliding Mode Control for Trajectory Tracking of Quadrotor Unmanned Aerial Vehicles Under Input Saturation and Disturbances. *Drones* **2024**, *8*, 614. <https://doi.org/10.3390/drones8110614>.
24. Tedesco, F.; Raimondo, D.M.; Casavola, A. Collision avoidance command governor for multi-vehicle unmanned systems. *Int. J. Robust Nonlinear Control* **2014**, *24*, 2309–2330. <https://doi.org/10.1002/rnc.2989>.
25. Yang, H.; Li, Q.; Zuo, Z.; Zhao, H. Event-triggered model predictive control for multi-vehicle systems with collision avoidance and obstacle avoidance. *Int. J. Robust Nonlinear Control* **2021**, *31*, 5476–5494. <https://doi.org/10.1002/rnc.5551>.
26. Bechlioulis, C.P. Robust Distributed Containment Control with Adaptive Performance and Collision Avoidance for Multi-Agent Systems. *Electronics* **2024**, *13*, 1439. <https://doi.org/10.3390/electronics13081439>.
27. Cong, Y.; Du, H.; Jin, Q.; Zhu, W.; Lin, X. Formation control for multiquadrotor aircraft: Connectivity preserving and collision avoidance. *Int. J. Robust Nonlinear Control* **2020**, *30*, 2352–2366. <https://doi.org/10.1002/rnc.4886>.
28. Babazadeh, R.; Selmic, R. Distance-Based Multiagent Formation Control With Energy Constraints Using SDRE. *IEEE Trans. Aerosp. Electron. Syst.* **2020**, *56*, 41–56. <https://doi.org/10.1109/TAES.2019.2910361>.
29. Katt, C.; Castañeda, H.; Castillo, P. Formation-Containment for a MAV Fleet Under Perturbations via Adaptive Sliding Mode Approach. In Proceedings of the 2021 International Conference on Unmanned Aircraft Systems (ICUAS), Athens, Greece, 5–18 June 2021; pp. 1530–1537. <https://doi.org/10.1109/ICUAS51884.2021.9476797>.
30. Zhu, Z.; Xia, Y.; Fu, M. Attitude stabilization of rigid spacecraft with finite-time convergence. *Int. J. Robust Nonlinear Control* **2011**, *21*, 686–702. <https://doi.org/10.1002/rnc.1624>.
31. Castañeda, H.; Gordillo, J.L. Spatial Modeling and Robust Flight Control Based on Adaptive Sliding Mode Approach for a Quadrotor MAV. *J. Intell. Robot. Syst.* **2019**, *93*, 101–111.

Disclaimer/Publisher’s Note: The statements, opinions and data contained in all publications are solely those of the individual author(s) and contributor(s) and not of MDPI and/or the editor(s). MDPI and/or the editor(s) disclaim responsibility for any injury to people or property resulting from any ideas, methods, instructions or products referred to in the content.